Supporting Information

Hamilton et al. 10.1073/pnas.1011558107

SI Materials and Methods

Slice Preparation. All animal procedures were performed in accordance with Canadian Council of Animal Care guidelines (protocol approved by the University of Alberta Health Sciences Laboratory Animal Committee) and relevant international laws and policies (EEC Council Directive 86/609, OJ L 358, 1, Dec. 12, 1987; Guide for the Care and Use of Laboratory Animals, US National Research Council, 1996).

Hippocampal slices were prepared from 3- to 5-wk-old male (or female where indicated) Sprague-Dawley rats as described previously (1, 2). Rats were decapitated and the brains were removed and placed into an ice-cold (0–4 °C) slicing solution containing (in mM): 124 NaCl, 3 KCl, 1.4 NaH_2PO_4, 1.3 $MgSO_4$, 26 $NaHCO_3$, 1.5 $CaCl_2$, 10 glucose, 1 kynurenic acid (Sigma), and saturated with 5% CO_2, 95% O_2 (carbogen). All extracellular solutions had an osmolarity of 300 ± 2 mOsm. Transverse slices (300 μM thick; ref. 2) were cut with a Slicer HR-2 (Sigmann-Elektronik) and placed in a 32–34 °C ACSF solution containing (in mM): 124 NaCl, 3 KCl, 1.4 NaH_2PO_4, 1.3 $MgSO_4$, 26 $NaHCO_3$, 1.5 $CaCl_2$, 10 glucose, and saturated with carbogen, for 15 min, then maintained at room temperature for an additional 30 min before initiating experiments.

Electrophysiology. Hippocampal slices were submerged in a continuous flow (2.5–3.5 mL/min) of ACSF at 33.0 ± 1.0 °C on the stage of an upright microscope (Axioskop FS2, Carl Zeiss). Dentate granule cells were visually identified with 20×, 40× (Carl Zeiss), or 60× (Olympus) water-immersion objectives and IR-differential interference contrast (DIC) optics. Whole-cell patch clamp recordings were obtained using borosilicate glass pipettes (4–6 MΩ) filled with an intracellular solution containing (mM): K-Glu-135, 7 KCl, 10 hepes, 10 Na-phosphocreatine, 4 Mg-ATP, 0.3 GTP, 10 EGTA (unless otherwise indicated), and 0.02% neurobiotin, pH 7.1–7.3, 292–296 mOsm. Recordings from DGCs were made using an Axoclamp 2A amplifier (Axon Instruments) in bridge current-clamp mode. APs were evoked with 1-ms square pulses of 1–5 nA current injected into the pipette in trains of 4–5 pulses with frequencies ranging from 20 to 200 Hz. Trains of synaptic stimuli were evoked with a stimulus intensity set to 50% of the maximal response (determined in individual stimulus–response curves for each DGC).

Calcium Imaging. Dentate granule cells in slices maintained as above were loaded with fluorescent Ca^{2+} indicator OGB-1 (Invitrogen) via the whole-cell pipette. The intracellular solution was the same as above, but containing (in mM): 0 EGTA, 0.1 $CaCl_2$, 0.1 OGB-1 (Invitrogen), and 0.001–0.01 Alexa 594. In most experiments, 30 min of OGB-1 loading was sufficient for Ca^{2+} signals to be measurable in dendrites up to 250 μm from the soma. Fluorescence was imaged with an image-intensified frame-transfer CCD camera (Pentamax, Princeton Instruments). Data were recorded using MetaFluor 6.3 (Molecular Devices) acquired at frame rates of 25–50 Hz. Changes in intracellular Ca^{2+} levels were determined offline by selecting ROIs along the dendrite of interest and subtracting background fluorescence from an average of two ROIs of equal dimensions in areas away from the neuron. $\Delta F/F$ was calculated by dividing the change in fluorescence (ΔF) by the fluorescence intensity before stimulation (F).

Immunohistochemistry. After recordings, slices were fixed in 4% buffered paraformaldehyde for at least 48 h then washed in a potassium phosphate buffer solution (KPBS) containing KH_2PO_4 (3.57 mM),K_2HPO_4 (anhydrous; 16.43 mM), and NaCl (15.4 mM), and dehydrated in 25% sucrose for 48–72 h. Slices were then incubated in streptavidin-conjugated Alexa 555 (Molecular Probes), 2% normal goat serum (Rockland), and 0.3% Triton X-100 (Sigma) for 2 h. After washout with KPBS, slices were mounted on slides with Prolong Gold antifade reagent (Invitrogen) and imaged with an upright confocal microscope (LSM 510, Carl Zeiss).

Drugs. For bath application, all drugs and peptides were dissolved in ACSF and perfused on slices at a flow rate of 2.5–3.5 mL/min. Human NPY (hNPY) was purchased from Peptidec Technologies. The receptor preferring agonists: [ahx^{5-24}]NPY, F^7P^{34}NPY, and [hPP^{1-17}, Ala^{31}, Aib^{32}]hNPY, were the generous gift of Prof. Annette Beck-Sickinger (Leipzig, Germany) and made by solid-state synthesis, as described previously (2). In some experiments, different cominations of the following were applied via the bath as indicated: 50 μM DL-2-Amino-5-phosphovaleric acid (APV; Tocris), 1 mM kynurenic acid (Sigma), 100 μM picrotoxin (Sigma), 50 μM cadmium chloride (Sigma), 5 μM nifedipine (Sigma), 5 μM ω-conotoxin-GVIA (Sigma), 10 μM D1R agonist SKF 81297 hydrobromide (Tocris), and dibutyrl cAMP (db-cAMP;10 μM; Tocris). All K^+ channel toxins were obtained from Alomone Laboratories (Jerusalem), except correolide (generous gift of Dr. Don Marsh, Merck Research Laboratories, Rahway, NJ) and 4-AP (Sigma). Local application experiments were performed using borosilicate glass pipettes (1–2 MΩ) filled with ACSF containing the compound of interest and 0.5–1 μM of Alexa 594 to visualize the application.

Theta-Burst Pairing Protocol. The theta-burst pairing protocol involved the pairing of a medial perforant path EPSP with an action potential (EPSP-action potential; 5-ms interval; Fig. 4*B*). Ten trials, each consisting of five EPSP-action potential pairs at 100 Hz, were repeated eight times at theta frequency (5 Hz). Stimulus-intensity response curves for EPSP amplitude were constructed before TBP, and stimuli set to 50% maximum used to evoke EPSPs for the remainder of the experiment. EPSPs were recorded as an average of five successive sweeps (5-s interstimulus interval) once every minute. All DGCs were in the inner or middle GCL.

Statistical Analysis. All data presented are as mean ± SEM unless otherwise indicated, with "*n*" being the number of neurons analyzed. For comparisons of group values repeated measures one- and two-way ANOVAs were performed with Bonferroni's multiple comparison test. Student's paired or unpaired *t* tests were also used with alpha values of 0.05 for small data sets. One-sample *t* tests were used to compare means with a hypothetical value of 0 or 100 as appropriate. Pearson correlations were calculated with two-tailed *P* values.

Human Brain Slices. Slices of human dentate gyrus were prepared from biopsies obtained during surgical resection from 10 female patients (35–62 y old) and one male patient (36 y old) with medically intractable temporal lobe epilepsy, under a protocol approved by the Health Research Ethics Board of the University of Alberta and Capital Health Authority. Transverse slices containing hippocampus were cut at 350–400 μM within 5 min of tissue biopsy. All other procedures were the same as in experiments with rat tissue.

1. Klapstein GJ, Colmers WF (1997) Neuropeptide Y suppresses epileptiform activity in rat hippocampus in vitro. *J Neurophysiol* 78:1651–1661.

2. El Bahh B, et al. (2005) The anti-epileptic actions of neuropeptide Y in the hippocampus are mediated by Y and not Y receptors. *Eur J Neurosci* 22:1417–1430.

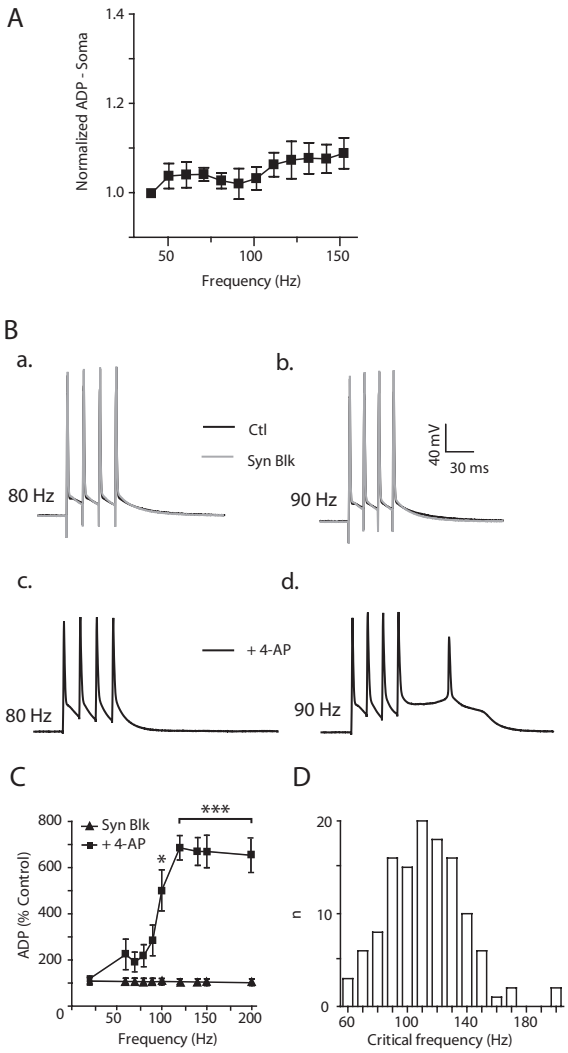

Fig. S1. 4-AP unmasks critical frequencies in DGCs. (*A*) Trains of four somatic action potentials (APs; 40–150 Hz) had no effect on the time-voltage integral of the after-depolarization (ADP) recorded at the soma. However, simultaneous Ca^{2+} transients in the distal dendrites showed a frequency-dependent response (Fig. 1 *E*–*G*). (*B*) Trains of APs at 80 Hz (*a* and *c*) and 90 Hz (*b* and *d*) evoked in a DGC with somatic current pulses (1 ms) with synaptic transmission blocked (Syn Blk; picrotoxin, 100 μM; APV, 50 μM; kynurenic acid, 100 μM; and increased Mg^{2+}, to 5 mM; *a* and *b*). With the addition of 4-AP (100 μM; *c* and *d*), the ADP increased above the CF (90 Hz, in this DGC). Somatic ADPs were quantified by calculating the time-voltage integral from the onset of the last action potential in the train to the return of the membrane potential to baseline. (*C*) The time-voltage integral shows no change relative to control conditions (% control) in the presence of the synaptic blockers alone, but with the addition of 4-AP (100 μM) the ADP integral increases sharply at upper frequencies. (*$P < 0.05$, **$P < 0.01$, ***$P < 0.001$; $n = 16$). (*D*) The distribution of CFs in the presence of 100 μM 4-AP resembles a normal distribution ($n = 138$).

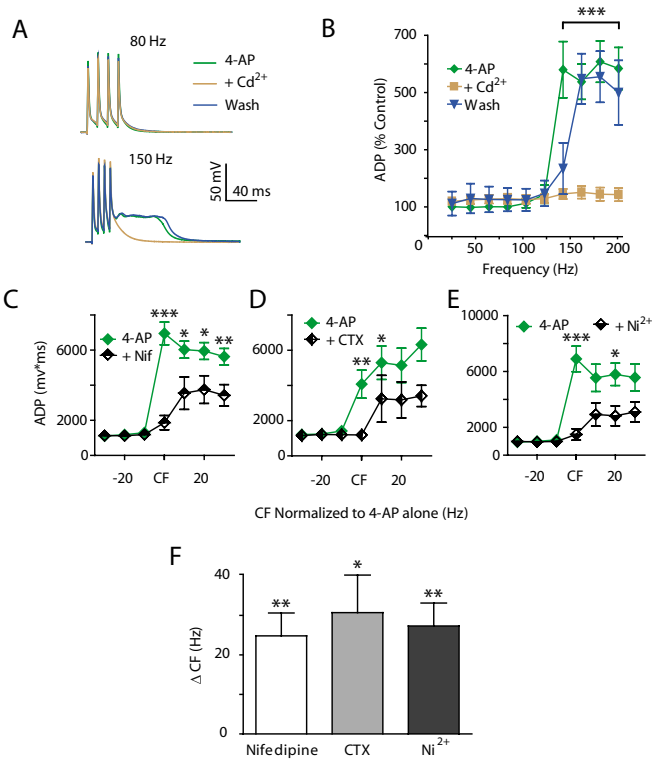

Fig. S2. The ADP is inhibited and critical frequencies are shifted by voltage-dependent Ca^{2+} channel blockers. (*A*) Cadmium (Cd^{2+}; 50 μM) inhibited the ADP elicited in the presence of 4-AP (100 μM) at higher frequencies, but had no measureable effect at frequencies below the CF. (*B*) Cadmium abolishes the frequency-dependent increase in ADP integral unmasked with 4-AP (100 μM), across all supracritical frequencies (***$P < 0.001$; $n = 12$) (*C–E*). Nifedipine (5 μM; $n = 9$), ω-conotoxin GVIA (CTX; 5 μM; $n = 6$), and nickel (50 μM; $n = 9$) significantly reduced the ADP observed at, and above, the 4-AP (100μM)-induced CF (*$P <$ 0.05, **$P < 0.01$, ***$P < 0.001$; $n = 5$). (*F*) Mean change in CF (ΔCF) for nifedipine (5 μM; 25 ± 6 Hz; $n = 9$), CTX (5 μM; 31 ± 10 Hz; $n = 6$), and nickel (50 μM; 27 ± 6 Hz; $n = 9$) were all significantly different from zero (*$P < 0.05$, **$P < 0.01$).

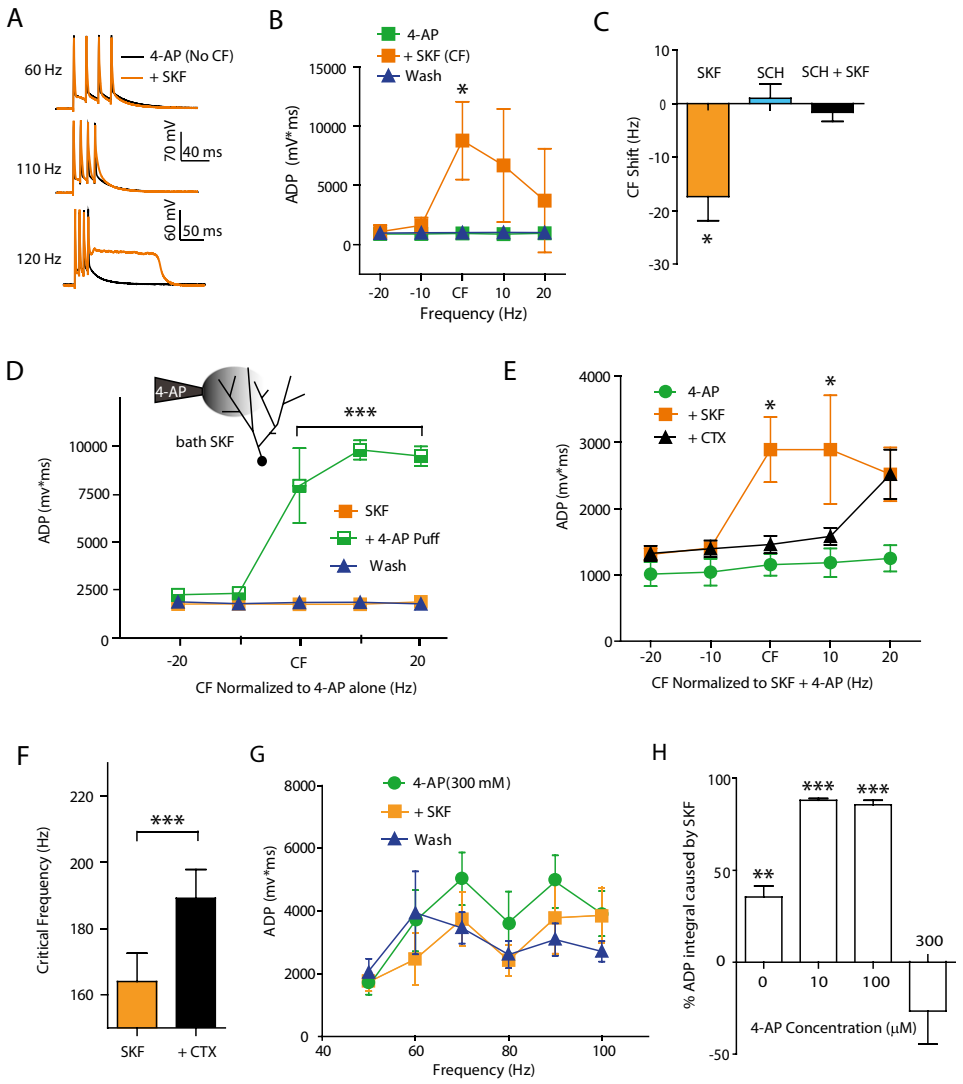

Fig. S3. D1 receptors mediate actions similar to 4-AP, by causing increased activity-dependent Ca^{2+} influx into DGC dendrites. (*A*) Some DGCs did not show a CF in the presence of 10 μM 4-AP alone. However, additional application of SKF 81297 (SKF, 10 μM) resulted in reversible unmasking of robust ADPs at and above a clear CF. (*B*) In DGCs that did not show a CF when bathed in 10 μM 4-AP, coapplication of SKF induced an ADP, unmasking a CF, and elevating ADP responses at several higher frequencies; this response reversed upon washout of SKF ($n = 4$). (*C*) SKF (10 μM) significantly left-shifted the CF (-17 ± 4 Hz; $^*P < 0.05$; $n = 5$) in DGCs in the presence of 4-AP (100 μM). After washout of SKF, application of the D1 antagonist SCH 23390 (2 μM) had no effect on the CF (CF shift: 1 ± 3 Hz; $P > 0.7283$; $n = 5$), but blocked the effects of subsequent coapplication of SKF with SCH present. (CF shift: -2 ± 2 Hz; $P > 0.405$; $n = 5$). (*D*) In DGCs that did not exhibit a detectable ADP when bathed with SKF (10 μM), focal (pressure) application of 4-AP (100 μM) to the distal dendrites (>140 μm from the soma) unmasked a reversible CF (152 ± 4 Hz; $n = 4$). Location of application was visualized with addition of Alexa 594 (500 nM) to the 4-AP solution in the puffer pipette; DGCs were also filled with Alexa 594 (10 μM) via the intracellular pipette (also Fig. 2*C*). In these experiments synaptic transmission was blocked (picrotoxin, 100 μM; APV, 50 μM; kynurenic acid, 100 μM; and Mg^{2+} increased to 5 mM). ***SKF vs. 4-AP Puff, $P < 0.001$; $n = 4$. (*E*) In DGCs that did not show a CF in the presence of 10 μM 4-AP, coapplication of SKF induced an ADP and a clear CF. Subsequent coapplication of CTX (1 μM) with SKF reduced the ADP integral at, and 10 Hz above, the SKF-induced CF ($^*P < 0.05$; $n = 5$). (*F*) A significant increase was caused by the CF unmasked by SKF (164 ± 9 Hz) when CTX was added (189 ± 9 Hz; $^{***}P < 0.001$; $n = 5$) (*G*) Trains of somatic action potentials at frequencies from 50 to 150 Hz evoked large ADPs in the presence of a high concentration of 4-AP (300 μM, not illustrated). The application of SKF did not change the ADP integral ($n = 6$) or the CF under these conditions. (*H*) The percentage of the ADP integral caused by SKF in similar experiments either without 4-AP or in the presence of the indicated 4-AP concentrations was calculated by dividing the ADP integral in the presence of SKF by the ADP integral either in control saline (for "0 μM 4-AP") or in the indicated concentrations of 4-AP immediately before application of the D1 agonist. (0 μM 4-AP, $n = 6$; 10 μM 4-AP, $n = 4$; 100 μM 4-AP, $n = 8$; 300 μM 4-AP, $n = 6$; $^{**}P < 0.01$, $^{***}P < 0.001$).

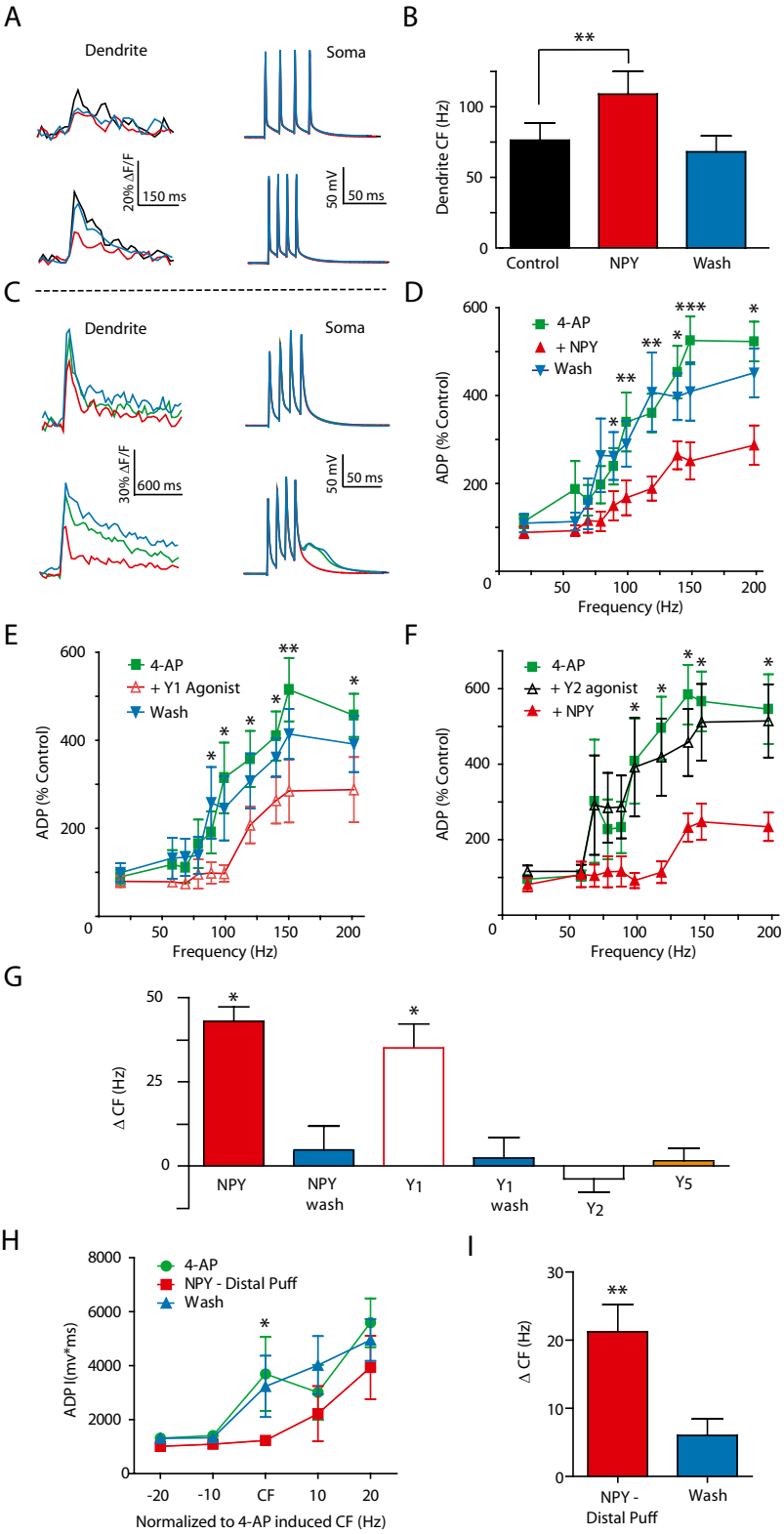

Fig. S4. NPY inhibits the ADP, distal dendrite Ca^{2+} currents, and shifts the CF both with bath and focal application to distal DGC dendrites. (*A*) DGCs were filled with OGB-1 via the patch pipette and distal Ca^{2+} influx was recorded as % $\Delta F/F$. Trains of four bAPs (40–200 Hz) were evoked and recorded electrically as before. Responses at 70 Hz (*Upper*) and 100 Hz (*Lower* traces) are shown. In the absence of 4-AP, measurements of distal Ca^{2+} influx (dendrite, *Left* traces) demonstrated a CF whereas no CF was seen at the soma (*Right* traces). The amplitude of the dendritic Ca^{2+} transients was decreased by NPY(red line) and returned to control levels with washout (blue line) in the dendrite. (*B*) Summary of experiments in the absence of 4-AP. NPY shifted the mean CF significantly in the distal dendrites (**$P < 0.01$; $n = 5$). (*C*) A subcritical (90 Hz, *Upper*) and a supracritical train (100 Hz, *Lower* traces) recorded at the soma and distal dendrite as in *A* in the presence of 4-AP (100 μM; green line). NPY application inhibits both the distal Ca^{2+} current and somatic ADP above the CF (red line) and reverses

Legend continued on following page

with washout (blue line). (*D*) In pharmacological experiments, NPY and receptor-preferring agonists (all at 1 μM) were bath applied to DGCs in which 4-AP (100 μM) unmasked somatic ADPs (solid green squares). NPY (solid red triangles) decreases the ADP (n = 8) and reverses on washout (solid blue triangles; * P < 0.05, ** P < 0.01, *** P < 0.001, n = 6). (*E*) The Y1 agonist (F^7P^{34}NPY; open red triangles) decreases the ADP like NPY itself does (*D*) and also reverses on washout (solid blue triangles). Asterisk denotes a significant difference between 4-AP alone and with Y1 agonist (n = 10; *P < 0.05, **P < 0.01). (*F*) The Y2 agonist ([ahx$^{5\text{-}24}$]NPY; open black triangles) has no effect on the ADP with 4-AP present (n = 9). After Y2 agonist application, NPY(solid red triangles) had its usual effect (paired t test, *P < 0.05; n = 4). (*G*) Change in CF for all compounds applied in *D–E*, with washout of the active agonists also shown. The Y5 agonist [hPP$^{1\text{-}17}$, Ala^{31},Aib^{32}]hNPY (1 μM), was without effect. (*P < 0.05). (*H*) In the presence of 4-AP (100 μM), the ADP was recorded in DGCs filled with Alexa 594 (1 μM). NPY (3 μM) was applied focally from a puffer pipette also containing Alexa 594 (500 nM). Distal application of NPY (>100 μM from the soma) significantly, and reversibly inhibits the ADP integral at the CF (*P < 0.05; n = 5). (*I*) Distal application of NPY also significantly increases the CF (NPY: 21 ± 4 Hz; washout: 6 ± 2 Hz; *P < 0.05; n = 5).

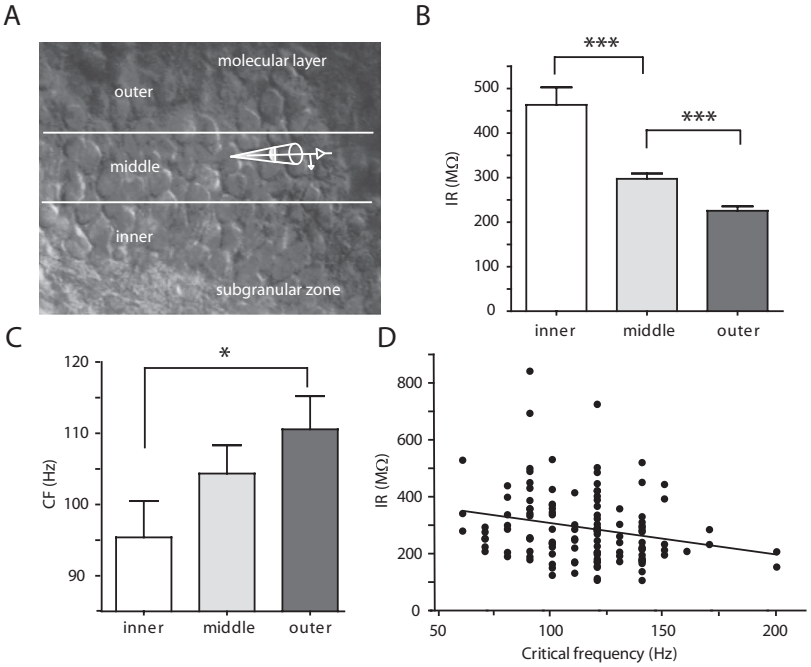

Fig. S5. CF varies with location of a DGC within the granule cell layer. Because there is an ongoing recruitment of new DGCs from the subgranular zone into the relatively mature granule cell layer, and young DGCs differ from mature ones in their excitability (3), we examined whether the CFs varied with DGC maturity. (*A*) We compared the input resistance (IR) of neurons in three visually defined regions of the granule cell layer (GCL): the inner third (adjacent to the hilus), middle third, and outer third (adjacent to the molecular layer). Pipette indicates one neuron in the middle layer. (*B*) Although previous studies classified subpopulations of DGCs on the basis of their electrophysiological properties as either "mature" (IR between 0.1 and 1 GΩ) or "young" (IR between 1 and 10 GΩ; ref. 1), our studies focused on cells within the GCL and not in the subgranular zone. As we rarely saw a neuron with an IR greater than 1 GΩ, the population we studied would be primarily mature DGCs. Nevertheless, even within this population of mature neurons within the GCL, IR decreased significantly in DGCs with somata in the outer third vs. the inner third (outer: 225.6 ± 9.9 MΩ, n = 68; middle: 297.4 ± 11.8 MΩ, n = 117; inner: 463.5 ± 39.5 MΩ, n = 58; ***P < 0.001). This is consistent with the postulated maturation of DGCs in a gradient from the inner to outer GCL (2). (*C*) We next compared the CFs in neurons from the three regions of the GCL as above. In the presence of 4-AP, the outermost granule cells (those with the lowest IR) had a significantly higher CF than did DGCs in the innermost granule cell layer (outer: 116 ± 5 Hz, n = 36; middle: 109 ± 4 Hz, n = 76; inner: 100 ± 5 Hz, n = 26; *P < 0.05). (*D*) CFs were binned by 10-Hz intervals and plotted against IR. There was a small, but significant correlation between input resistance and CF (r^2 = 0.05, n = 127).

1. Schmidt-Hieber C, Jonas P, Bischofberger J (2004) Enhanced synaptic plasticity in newly generated granule cells of the adult hippocampus. *Nature* 429:184–187.
2. Piatti VC, Espósito MS, Schinder AF (2006) The timing of neuronal development in adult hippocampal neurogenesis. *Neuroscientist* 12:463–468.

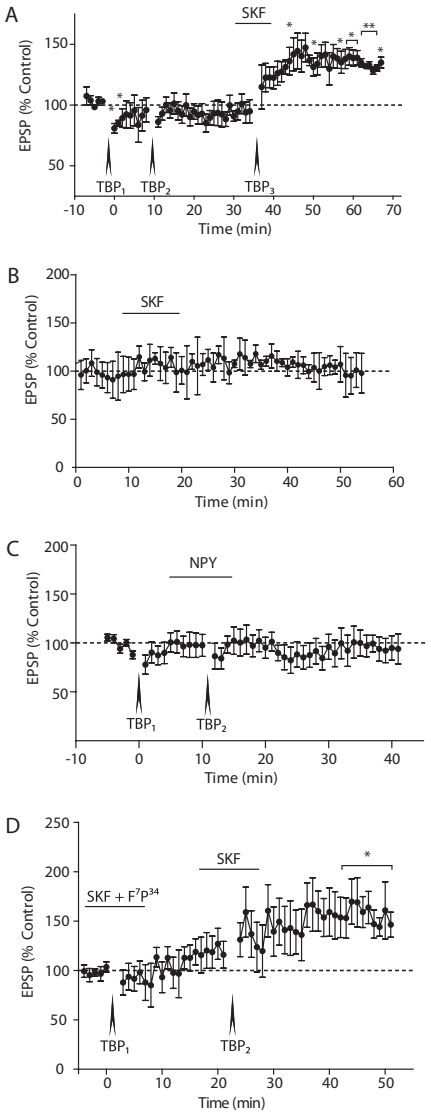

Fig. S6. TBP only induces LTP in the presence of SKF. (*A*) TBP_1 followed by TBP_2 (both in control saline) did not cause LTP; however, SKF (10 μM) application coupled with TBP_3 induced significant LTP (*$P < 0.05$, **$P < 0.01$; $n = 3$). (*B*) SKF (10 μM) without synaptic pairing does not induce LTP ($n = 3$). (*C*) NPY (1 μM) does not affect synaptic activity in the absence of D1 agonist ($n = 12$). (*D*) Synaptic pairing in the presence of the NPY1 agonist F^7P^{34} (1 μM) and SKF (10 μM) did not result in a change in EPSP amplitude 20 min after TBP_1. After both drugs had washed out for 15 min, SKF (10 μM) was applied alone. Under these conditions, TBP_2 induced LTP (*$P < 0.05$; $n = 5$).

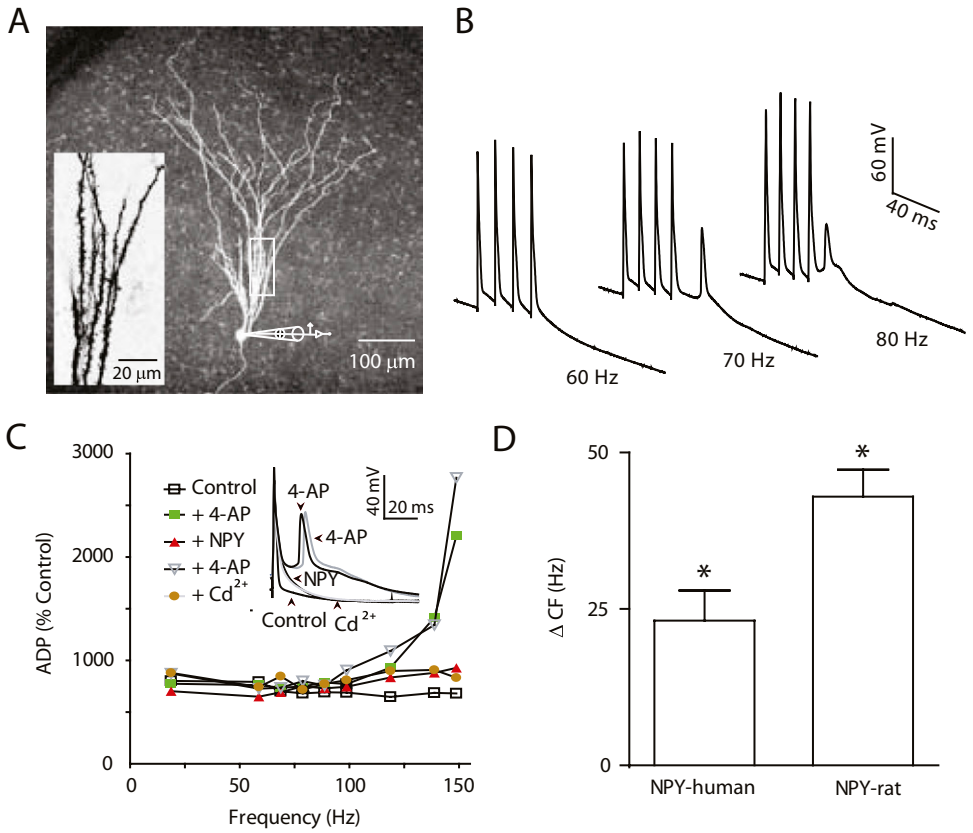

Fig. S7. NPY increases the CFs in human DGCs. (*A*) Neurobiotin-filled image of a human DGC. Example of the density of dendritic spines (*Inset*). (*B*) Response to trains of depolarizing current injections in human DGC in the presence of 100 μM 4-AP (responses to 60-, 70-, and 80-Hz trains are illustrated). (*C*) The ADP recorded in human DGCs in control (open black squares), in the presence of 4-AP (100 μM; solid green squares), and with the addition of NPY (1 μM; solid red triangles), which profoundly inhibited the ADP. Following washout of NPY with 4-AP solution (open gray triangles) and recovery of the ADP, Cd^{2+} (50 μM; solid yellow circles) again inhibited the ADP. (*Inset*) Voltage traces after 150 Hz stimulation under the above conditions. (*D*) NPY caused a significant, reversible CF change when applied to human DGCs (*$P < 0.05$; $n = 6$).

Table S1. The effect of various K^+ channel blockers on the CF and ADP

Drug	Channel(s) blocked (IC_{50})	References	CF observed?	Increase in ADP observed?	*n*	Concentration used
4-Aminopyridine	K_v 1.4 (160 μM) Kv 1.5 (50 μM) K_v 3.1–3.2 (0.02–0.5 mM) K_v 4.2 (1.5 mM)	Alexander et al. (1); Rudy and McBain (2); Tseng et al. (3); Bouchard and Fedida (4)	Yes	Yes	>200	100 μM
α-Dendrotoxin	K_v 1.1 (4 nM) K_v 1.2 (12 nM) K_v 1.6 (25 nM)	Alexander et al. (1); Harvey (5)	No	No	5	500 nM
Correolide	K_v 1.1 (430 nM) K_v 1.2 (700 nM) K_v 1.3 (86 nM) K_v 1.4 (<1100 nM) K_v 1.5 (1150 nM) K_v 1.6 (450 nM)	Felix et al. (6)	No	No	5	10 μM
rStichodactyla toxin (ShK)	K_v 1.1 (1 pM), K_v 1.3 (1 pM), K_v 1.4 (<1 nM), K_v 1.6 (<1 nM), K_v 3.2 (6 nM)	Middleton et al. (7); Yan et al. (8)	No	No	4	500 nM
Paxilline	K_{Ca} 1.1 (BK or Maxi-K; 300 nM)	Saleem et al. (9); Brenner et al. (10)	No	No	8	5 μM
Apamin	K_{Ca} 2.1 (10 nM) K_{Ca} 2.2 (3 nM) K_{Ca} 2.3 (<1 nM)	Alexander et al. (1); Gauldie et al. (11); Logsdon et al. (12); Shah and Haylett (13)	No	No	8	1 μM
Charybdotoxin	K_v 1.2 (6 nM) K_v 1.3 (20 nM) K_{Ca} 3.1 (30 nM)	Spunger et al. (14); Alexander et al. (1); Van Renterghem et al. (15), 1995; Yao et al. (16)	No	No	5	50 nM
Phrixotoxin-1	K_v 4.2 (70 nM), K_v 4.3 (5 nM)	Diochot et al. (17)	No	No	5	200 nM
TEA	K_v 1.1 (0.5 mM) K_v 1.3 (1 mM) K_v 1.6 (0.6 mM) K_v 2.1 (2.9 mM) K_v 2.2 (2.6 mM) K_v 3.1–3.4 (200–300 nM) $KCNQ_1$ (5 mM) $KCNQ_2$ (0.3 mM) $KCNQ_3$ (>30 mM) $KCNQ_4$ (3 mM)	Alexander et al. (1); Hadley et al. (18); Thornhill et al. (19); Shevchenko et al. (20)	No	No	6	1 mM

Somatic action potentials were evoked in trains of frequencies from 50 to 200 Hz in the presence of the Syn Blk solution (containing 100 μM picrotoxin, 1 mM kynurenic acid, 50 μM APV, and Mg^{2+} elevated to 5 mM). All compounds were applied by the bath at the given concentrations. Critical frequencies and increased after-depolarizations were only observed in the presence of 4-AP.

1. Alexander SPH, Mathie A, Peters JA (2008) Guide to receptors and channels (GRAC), 3rd edition. *Br J Pharmacol* 153(Suppl 2):S1–S209.
2. Rudy B, McBain CJ (2001) Kv3 channels: Voltage-gated K+ channels designed for high-frequency repetitive firing. *Trends Neurosci* 24:517–526.
3. Tseng GN, Jiang M, Yao JA (1996) Reverse use dependence of Kv4.2 blockade by 4-aminopyridine. *J Pharmacol Exp Ther* 279:865–876.
4. Bouchard R, Fedida D (1995) Closed- and open-state binding of 4-aminopyridine to the cloned human potassium channel Kv1.5. *J Pharmacol Exp Ther* 275:864–876.
5. Harvey AL (2001) Twenty years of dendrotoxins. *Toxicon* 39:15–26.
6. Felix JP, et al. (1999) Identification and biochemical characterization of a novel nortriterpene inhibitor of the human lymphocyte voltage-gated potassium channel, Kv1.3. *Biochemistry* 38:4922–4930.
7. Middleton RE, et al. (2003) Substitution of a single residue in Stichodactyla helianthus peptide, ShK-Dap22, reveals a novel pharmacological profile. *Biochemistry* 42:13698–13707.
8. Yan L, et al. (2005) Stichodactyla helianthus peptide, a pharmacological tool for studying Kv3.2 channels. *Mol Pharmacol* 67:1513–1521.
9. Saleem F, Rowe IC, Shipston MJ (2009) Characterization of BK channel splice variants using membrane potential dyes. *Br J Pharmacol* 156:143–152.
10. Brenner R, et al. (2005) BK channel beta4 subunit reduces dentate gyrus excitability and protects against temporal lobe seizures. *Nat Neurosci* 8:1752–1759.
11. Gauldie J, Hanson JM, Rumjanek FD, Shipolini RA, Vernon CA (1976) The peptide components of bee venom. *Eur J Biochem* 61:369–376.
12. Logsdon NJ, Kang J, Togo JA, Christian EP, Aiyar J (1997) A novel gene, hKCa4, encodes the calcium-activated potassium channel in human T lymphocytes. *J Biol Chem* 272: 32723–32726.
13. Shah M, Haylett DG (2000) The pharmacology of hSK1 Ca2+-activated K+ channels expressed in mammalian cell lines. *Br J Pharmacol* 129:627–630.
14. Sprunger LK, Stewig NJ, O'Grady SM (1996) Effects of charybdotoxin on K+ channel (KV1.2) deactivation and inactivation kinetics. *Eur J Pharmacol* 314:357–364.
15. Van Renterghem C, Vigne P, Frelin C (1995) A charybdotoxin-sensitive, Ca(2+)-activated K+ properties and activation by endothelins. *J Neurochem* 65:1274–1281.
16. Yao X, et al. (2000) Close association of the N terminus of Kv1.3 with the pore region. *J Biol Chem* 275:10859–10863.
17. Diochot S, Drici MD, Moinier D, Fink M, Lazdunski M (1999) Effects of phrixotoxins on the Kv4 family of potassium channels and implications for the role of Ito1 in cardiac electrogenesis. *Br J Pharmacol* 126:251–263.
18. Hadley JK, et al. (2000) Differential tetraethylammonium sensitivity of KCNQ1-4 potassium channels. *Br J Pharmacol* 129:413–415.
19. Thornhill WB, et al. (1996) Expression of Kv1.1 delayed rectifier potassium channels in Lec mutant Chinese hamster ovary cell lines reveals a role for sialidation in channel function. *J Biol Chem* 271:19093–19098.
20. Shevchenko T, Teruyama R, Armstrong WE (2004) High-threshold, Kv3-like potassium currents in magnocellular neurosecretory neurons and their role in spike repolarization. *J Neurophysiol* 92:3043–3055.

Table S2. Comparison of DGC properties in male and female rats and female humans

	Male rat (n = 138)		Female rat (n = 16)		Human female (n = 18)	
	Mean	SE	Mean	SE	Mean	SE
RMP (mV)	−74.1	0.3	−74.7	1.2	−68.8*	1.2
IR (MΩ)	316.9	12.6	297.3	29.2	283.9	28.8
CF (Hz)	109	3	97	7	111	5

*Significant difference from both male and female rats, both $P < 0.05$.